Composites Part B 174 (2019) 106991

Contents lists available at ScienceDirect

Composites Part B

journal homepage: www.elsevier.com/locate/compositesb

3D-printed polymer composites with acoustically assembled multidimensional filler networks for accelerated heat dissipation

Lu Lu [a], Zhifeng Zhang [b], Jie Xu [a], Yayue Pan [a,*]

[a] Department of Mechanical and Industrial Engineering, University of Illinois at Chicago, Chicago, IL, 60607, USA
[b] Department of Engineering Science and Mechanics, Pennsylvania State University, State College, PA, 16802, USA

ARTICLE INFO

Keywords:
Additive manufacturing
Functional polymer composites
Filler network
Composite design
Heat dissipation

ABSTRACT

Polymer composites containing thermally conductive fillers show great promise in solving the overheating issue which is critical for electronic devices. Recent successes in developing functional polymer composites rely on the excellent filler property and heavy loading. Yet the intensive filler loading leads to challenges in manufacturing and composite properties. This study reports an alternative method for functional particle-polymer composite design and fabrication: instead of heavy loading, a small amount of filler composes highly concentrated multi-dimensional network functioning as active paths for heat dissipation in the polymer matrix. A novel 3D printing technique named acoustic field-assisted projection stereolithography realizes the fabrication of such composites. The local filler weight ratio in the network is > 7 times of the feedstock filler loading. With the same feedstock, the patterned composite exhibits >10 times higher efficiency in heat dissipation, compared to the uniform composite. With the same amount of fillers embedded, the patterned composite accelerates the heat dissipation twice than the uniform composite. Moreover, 3D filler network outperforms 2D network, showing that the higher network dimension is conducive to multidirectional heat transfer. With a low filler consumption while higher design flexibility, this new composite material design and manufacturing approach overcomes restriction caused by filler loading.

1. Introduction

Heat dissipation speed directly affects electronic device lifetime and reliability by proactively preventing degradation and failure caused by overheating. A survey from the U.S. Air Force reports that more than 50% of electronics failures are caused by overheating [1]. 1 °C reduction in component operation temperature leads to 4% decrease in its failure rate [2]. Therefore, thermal management is a primary concern for the current generation of electronic devices and will become increasingly critical. In advanced application fields such as 3D chipsets, wearable devices, and flexible electronics, now more than ever there are both needs and opportunities for novel structures and materials to help address thermal challenges.

Being thermally conductive, mechanically flexible, and electrically insulated, polymer composites with synergistic inclusion of thermally conductive fillers show promises as an emerging material for thermal management applications [3–10]. The conventional method of fabricating polymer composites is randomly distributing functional fillers in the polymeric matrix through mixing or milling [11]. Although several articles have demonstrated significant thermal property improvements by introducing a heavy filler loading (30–70 wt%), the heavy filler loading usually brings manufacturing challenges, such as clogging, difficulty in mixing, agglomeration, trouble in filler embedding, and limitation of manipulating the filler local distributions and orientations in the polymer matrix. Additionally, the manufactured composites with heavy filler loading usually suffer from insufficient binding, mechanical deterioration, and thermal expansion coefficient mismatch [12–15]. The disordered distribution of fillers limits thermal performance enhancement due to the phonon scattering between isolated fillers [16]. Instead of uniformly distributing a massive amount of functional fillers in the polymer matrix, here we propose to construct composites by forming and embedding interconnected filler networks in the polymer matrix, using feedstock of a low filler loading fraction and a multi-material Additive Manufacturing (AM) technology.

With the capability of locally controlling the filler alignment, orientation, and concentration, multi-material AM can enable higher design flexibility of novel composites [17–20]. Many AM processes have been explored to produce such filler-polymer composites, such as

* Corresponding author. Department of Mechanical and Industrial Engineering, University of Illinois at Chicago, 842 W Taylor St, ERF 1076, Chicago, IL, 60607
E-mail address: yayuepan@uic.edu (Y. Pan).

https://doi.org/10.1016/j.compositesb.2019.106991
Received 29 April 2019; Received in revised form 20 May 2019; Accepted 27 May 2019
Available online 31 May 2019
1359-8368/

stereolithography (SL) [21], fused deposition modeling (FDM) [22], direct ink writing [23], selective laser sintering (SLS) [24], ink-jet printing [25], and selective laser melting (SLM) [26]. Filler manipulation approaches including methods based on shear-flow [27], electrical field [28], magnetic field [19,20], and acoustic field [29–31] have been explored to integrate with AM for fabricating polymer composites with locally controlled filler distributions or orientations.

Compared to other methods, acoustic-field-based filler manipulation technique has many unique advantages including full filler distribution control, no enforced manufacturing restriction, and no filler shape and property requirements [32–34]. Integration of the acoustic field with AM has been reported in a few studies. Llewellyn-Jones et al. utilized an acoustic field to align glass fibers in the polymer matrix, but experienced difficulties in multiple layer fabrication [29]. Yunus et al. employed the acoustic field to form lines of electrically conductive particles for electronic applications [30]. They investigated the impact of functional fillers and filler concentrations on part performance. To the best knowledge of authors, no study has been reported on the effects of acoustic assemblies and filler network geometries on composite performance. This study is aimed to explore these effects with a focus on the heat dissipation performance of the 3D printed composites.

In this work, the acoustic field assisted projection stereolithography (A-PSL) process is developed to fabricate polymer composites with two-dimensional (2D) and three-dimensional (3D) filler assembly networks. Impacts of the acoustic assembly and the filler network on heat dissipation are investigated. The rest of the paper is organized as follows: A-PSL process and filler patterning by A-PSL are introduced in section 2. Section 3 presents the design, material, and fabrication of composite samples. Details about the heat dissipation experiment and modeling are given in section 4.1. Sections 4.2 to 4.4 demonstrate experimental results and discuss the thermal performances of composites with varied filler network geometries. Conclusions and future work are summarized in the end.

2. Acoustic field assisted projection stereolithography for composites production

2.1. Manufacturing process overview

In the Acoustic Field Assisted Projection Stereolithography (A-PSL) process, the acoustic field assisted filler self-assembly mechanism is integrated into the bottom-up projection SL setup, as illustrated in Fig. 1a.

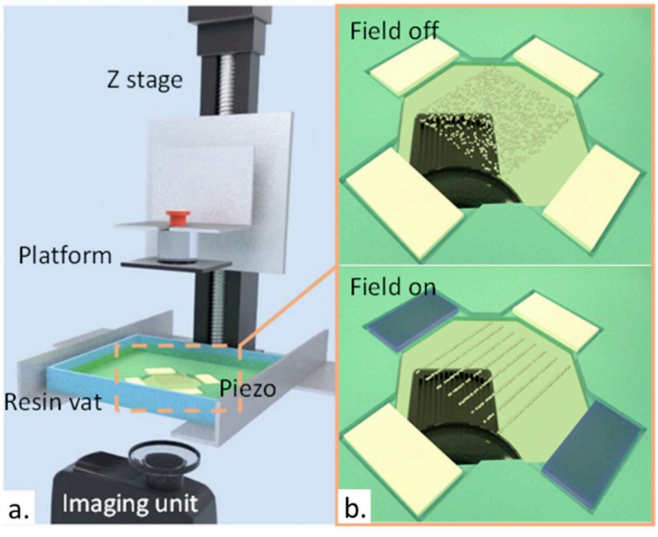

Fig. 1. The A-PSL setup: a. Schematics of A-PSL system; b. Schematics of the acoustic field assisted filler assembly.

Key components are an imaging unit, a resin vat, several piezo elements, and a platform driven by the Z stage. The resin vat holds the premixed resin-filler suspension. The printing process starts with slicing the 3D Computer Aided Design (CAD) model of the object to 2D layers. Then the sliced layers are converted into digital mask images. Next, the piezo elements are actuated, as highlighted in Fig. 1b by blue color, to generate the acoustic field in the suspension, resulting in the formation of filler patterns within a few seconds (~5 s). Once the filler assembly is formed, the Z stage drives the platform down until forming a one-layer thickness gap with the bottom surface of the resin vat. The imaging unit exposes a digital mask to solidify the suspension selectively. The exposure time is determined according to the loading fraction of the fillers. Curing time for suspensions with varied filler loading fractions has been modeled and characterized in our previous study [35]. Given a certain layer thickness, longer curing time is used for the suspension with a higher filler loading fraction. The cured part grows on the platform, in a layer-by-layer fashion. After curing of a layer, the piezo actuation is turned off, and the platform moves up for the resin to refill. Then, the suspension is mechanically stirred to achieve random distribution. By repeating these steps, a 3D composite object with desired filler distribution patterns can be fabricated. The projection SL provides geometric flexibility with fast build speed. The external acoustic field controls filler dispersion patterns and local material compositions.

To redistribute and assemble fillers, the acoustic field generation module composes of electro-piezo elements, a function generator, and an amplifier. The bottom surface of the resin vat is transparent. Four piezo plates are horizontally placed on each corner of the bottom. As the base of the resin vat, a transparent polyethylene terephthalate (PET) film is attached on the top of piezo plates. A function generator provides the sinusoidal signal with adjustable frequency and voltage. This signal is applied to the electro-piezo element after amplified. The piezo element actuation leads to structural deformation of the PET film, which subsequently induces an acoustic field in the filler-resin suspension. The acoustic radiation force drives fillers to the pressure nodes of the acoustic field to form a pattern.

2.2. Acoustic assembly of functional fillers in A-PSL process

In this study, one piezo plate was actuated to induce the formation of a parallel filler line pattern composed of the aluminum powder as demonstrated in Fig. 2a. The applied signal was set at a frequency of 44 kHz with a peak-to-peak voltage of 5 V. The line width is around 0.6 mm, and the space between lines is approximately 0.7 mm. After photo-curing, filler microstructures in line-pattern were locked inside the polymer matrix. Using 2.75 wt% suspension as feedstock, patterned samples with filler line embedded were prepared by A-PSL. For comparison, uniform composites were also fabricated using the same 2.75 wt % feedstock. Scanning electron microscope (SEM) images were taken from the side view of printed samples to observe the filler distribution in the uniform composite and the patterned composites. Due to the low filler loading fraction (2.75 wt%), the uniform composite contains only a few randomly distributed fillers and small filler clusters, as shown in Fig. 2b. In contrast, the patterned composite comprises dense and continuous filler network within each layer, as shown in Fig. 2c and d.

As characterized by SEM, the local filler weight ratio of the filler microstructure was measured to be ~20.5%, although the loading fraction in the feedstock is only 2.75 wt%. The height of the filler assembly is about 90 μm as marked in Fig. 2d. Therefore, to achieve sufficient interlayer filler contact, the printing layer thickness should be set to no larger than 90 μm.

3. Manufacturing of composites with varied filler distribution patterns

Heat diffuses slowly in the polymer matrix through Brownian motions [36], while in thermally conductive fillers it diffuses quickly as a

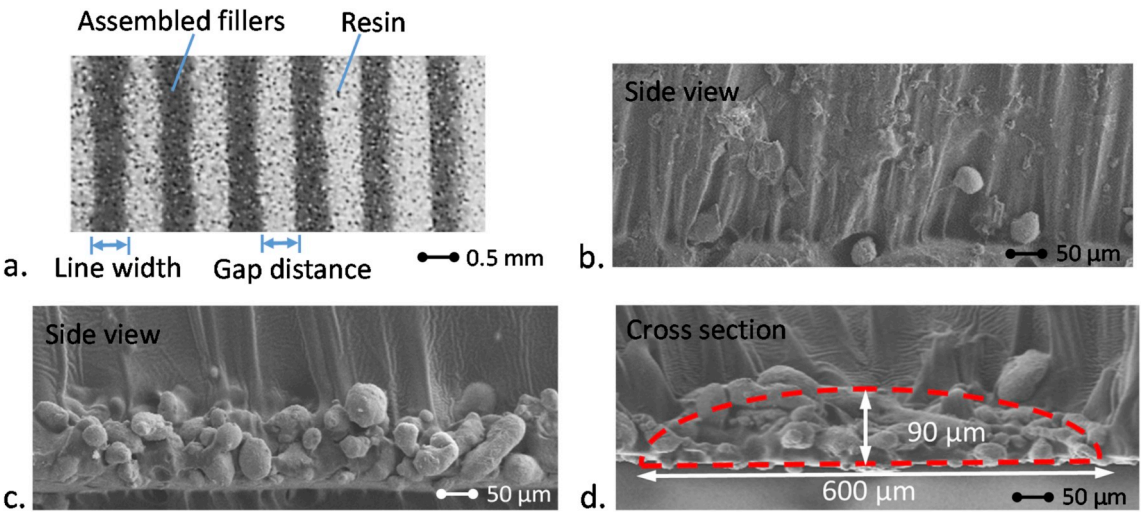

Figure 2. a. Photograph of parallel filler line pattern in liquid resin; SEM images of b. The uniform composite, c. The patterned composite, d. Acoustically assembled filler microstructure in cross-sectional view. (Filler: aluminum powder).

wave [37]. Compared to the uniform composite in which particles are discretely distributed, the assembled filler line in the patterned composite has a significantly reduced inter-particle distance. A smaller inter-particle distance requires less time for phonon to diffuse [36]. Hence, we hypothesized that the patterned composite exhibits a higher heat dissipation efficiency, compared to uniform composites fabricated from the same feedstock, and even uniform composites which comprised the same amount of functional fillers, as well as patterned composites

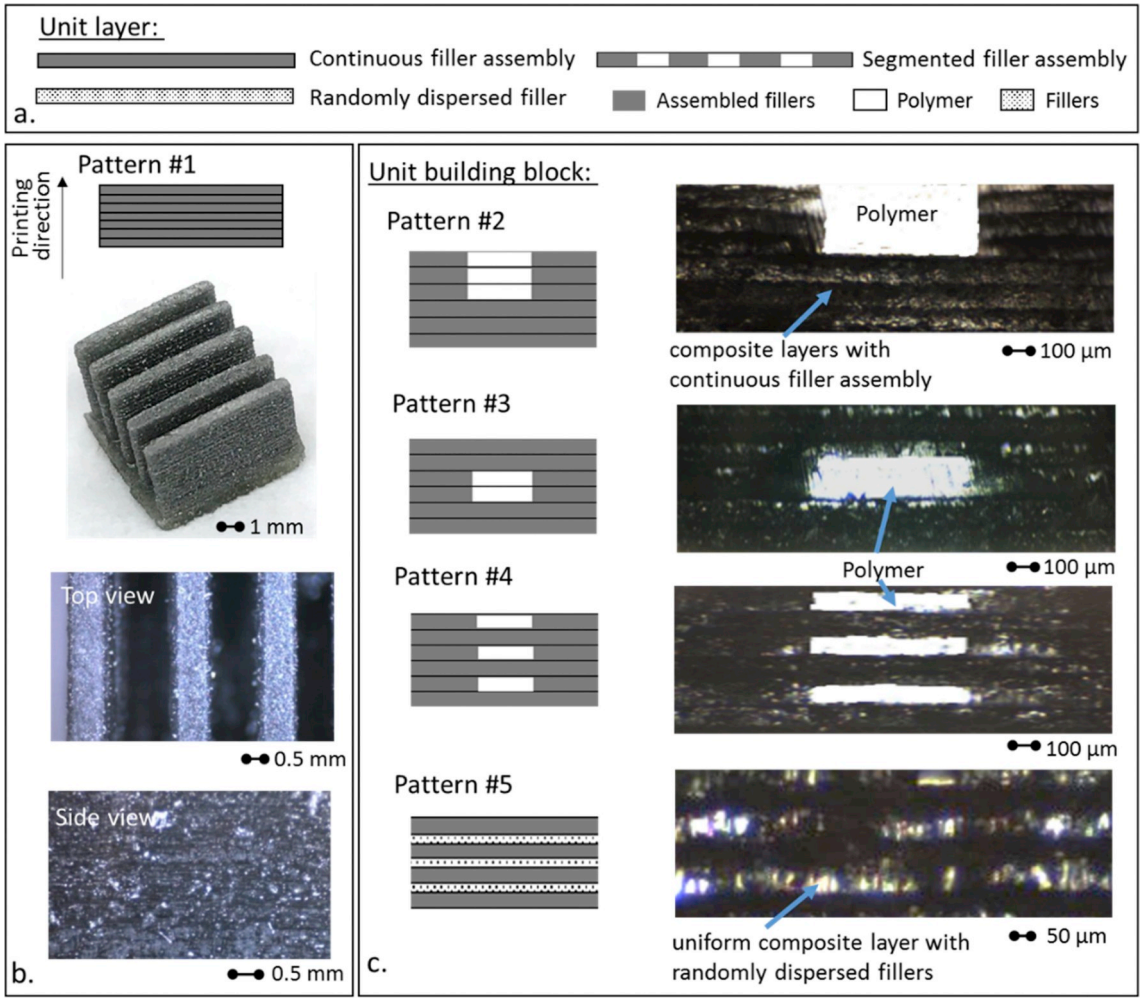

Fig. 3. a. Schematics of unit layers. b. Photograph of a printed sample P-1 and its microscopic images. c. Schematics of different filler distribution patterns and the microscopic images of fabricated samples in side views.

with a lower dimension of filler network constructed by the same amount of functional fillers.

To verify this hypothesis, a typical heat dissipation device, the heat sink with a fin width of 0.6 mm, was designed and printed using a layer thickness of 90 μm. The aluminum powder (Alpha Chemicals, MO, USA) was selected as the thermal functional filler. It is uncoated and produced through atomization. The particle size (D_{50}) is 30 μm. For easy observation purpose, a translucent color photopolymer resin, Spot-E Elastic (Sonnaya Ulitka S.L., Barcelona, Spain), was used as the base resin. Suspensions of the base resin and aluminum particles were prepared using a conditioning mixer (AR-100, Thinky, CA, USA), and were used as the feedstock for fabricating samples using the A-PSL setup.

The fabrication of patterned composites using A-PSL technique started with filler self-assembly in an appropriate acoustic field. Next, by selectively aligning the projection light with the acoustically formed filler lines, assembled filler microstructures were embedded into desired areas of the heat sink. All patterned composites were printed from the same feedstock with a filler loading fraction of 2.75 wt%. In this study, five different patterned composites were designed and fabricated. Three types of unit layers, the layer containing continuous filler assembly, the layer comprised of segmented filler assembly and the layer filled with randomly dispersed fillers are the basic building blocks for constructing different patterns. The schematic drawings in Fig. 3a demonstrate these unit layer types.

Sample P-1 comprises of continuous dense filler assembly in each layer of the fins. In Fig. 3b, the printed sample P-1 appears in gray owing to the inclusion of aluminum micro-particles. Moreover, a dark metallic color can be observed from microscopic images taken from the top view and side view. Sample P-2, P-3, and P-4 are composed of different filler distribution patterns along the printing direction achieved by combining two types of unit layers in various sequences as illustrated by the schematics and shown in the corresponding micro images of printed samples in Fig. 3c. For sample P-2, three layers of continuous filler assembly and three layers of segmented filler assembly appear in turn. Two layers of segmented assembly lines follow every two layers of continuous filler assembly in sample P-3. The layer of segmented filler assembly and the layer of continuous filler assembly were printed alternately in sample P-4. Each part was built with 15 layers of continuous filler assembly and 15 layers of segmented filler assembly. Sample P-5 was built by accumulating continues filler assembly layer and uniform composite layer alternately. The layer thickness of the uniform composite was set to be 45 μm to achieve the same as-fabricated filler loading fraction, 15.4 wt%, as samples P-2, P-3, and P-4.

As the comparison group, the second set of samples are parts filled with non-structured fillers. They were printed without utilizing the acoustic field. Uniform composites composed of 0 wt%, 2.75 wt%, 15.4 wt%, and 20.5 wt% fillers were printed using pure resin feedstock, and filler-resin suspensions with 2.75 wt%, 15.4 wt% and 20.5 wt% filler loading fractions, respectively. In these uniform composite samples, the content of fillers in the polymer matrix was determined by the filler loading fraction of the feedstock.

In this study, composites are named by Type(φ_{feed}, φ_{fab}), where Type is the composite material composition, which could be uniform composite U, type 1 patterned composite P-1, type 2 patterned composite P-2, type 3 patterned composite P-3, type 4 patterned composite P-4, and type 5 patterned composite P-5. φ_{feed} is defined as the filler loading fraction of the feedstock in weight ratio, and the as-fabricated filler loading fraction φ_{fab} is the weight of the filler content over the weight of the printed part. Details of all samples were summarized in Table 1. For the patterned composite sample set, φ_{fab} is much higher than φ_{feed} because fillers are redistributed and assembled into highly concentrated networks by the acoustic radiation force. By designing different patterns along the printing direction or selectively employing the acoustic field for specific layers, varied φ_{fab} can be achieved with a fixed φ_{feed}. On the contrary, φ_{fab} of uniform composite samples is strictly limited by φ_{feed}.

Table 1
Filler loading and distribution in printed samples.

SAMPLE: Type(ϕ_{feed}, ϕ_{fab})	ϕ_{feed} (WT %)	ϕ_{fab}(WT %)	Filler network dimension
U(0, 0)	0	0	–
U(2.75, 2.75)	2.75	2.75	1D
U(15.4, 15.4)	15.4	15.4	1D
U(17.5, 17.5)	17.5	17.5	1D
U(20.5, 20.5)	20.5	20.5	1D
P-5(2.75, 15.4)	2.75	15.4	2D
P-4(2.75, 15.4)	2.75	15.4	3D
P-3(2.75, 15.4)	2.75	15.4	3D
P-2(2.75, 15.4)	2.75	15.4	3D
P-1(2.75, 20.5)	2.75	20.5	3D

φ_{fab} of the uniform composite always equals to φ_{feed}. Hence, different from patterned composites, the adjustment of φ_{fab} for uniform composite parts can only be realized by changing φ_{feed} in the feedstock.

Samples are sorted according to the dimension of the filler network in Table 1. In uniform composites, fillers randomly dispersed in the polymer matrix. Therefore, the dimension of the filler network in uniform composites is defined as 1D, which represents no intimate connection between fillers. All patterned composite samples contain in-plane filler lines. In sample P-5(2.75, 15.4), uniform composite layer separates continuous filler assembly, resulting in disconnection of the filler network along the printing direction. This condition is defined as the 2D filler network. Through connecting 2D filler lines along the printing direction Z, substantial interlayer filler contacts are realized in samples P-1(2.75, 20.5), P-2(2.75, 15.4), P-3(2.75, 15.4) and P-4(2.75, 15.4), thus forming 3D filler networks. To fully understand the effects of acoustic assembly and filler networks on the heat dissipation efficiency, these fabricated composite samples were characterized and analyzed in the following sections.

4. Experiments and results

4.1. Cooling experiment and modeling

The cooling experiment was designed and conducted on the printed heat sinks to characterize the thermal performance, as illustrated in Fig. 4. A heat bed was set at 130 °C and used for heating heat sinks. Each heat sink was heated to 90 °C, and then was moved to a thermally isolated substrate at room temperature (25 °C). The dynamic heat transfer process of the heat sink was recorded and measured using a thermal imaging camera (FLIR Systems, Inc, OR, USA). The highest temperature detected on the heat sink was read from each frame.

To determinate the flow condition, we need to estimate the Rayleigh number (Ra), which is defined in terms of Prandtl number (Pr) and Grashof number (Gr), expressed by

$$Ra = Pr{*}Gr \tag{1}$$

where,

$$Gr = \mathrm{g} \times L_C^3 \times \beta \Delta T / \eta^2 \tag{2}$$

with g is acceleration of gravity, L_C is the characteristic length (~4 mm for fin in our experiment), β is the air thermal expansion coefficient (1/298, in K^{-1}), ΔT is the temperature difference between fin and the environment, η is the air kinetic viscosity ($\sim 1.5 \times 10^{-5}\ m^2/s$);

and,

$$Pr = \mu C_p / k_a \tag{3}$$

with μ is the air dynamic viscosity ($\sim 1.8 \times 10^{-5}\ kg/m{\cdot}s$), C_p is the specific heat of dry air (~1005 J/kg·K), k_a is air thermal conductivity (~0.026 W. m^{-1}. K^{-1}). With $Gr = 562$ and $Pr = 0.7$, we get $Ra =$

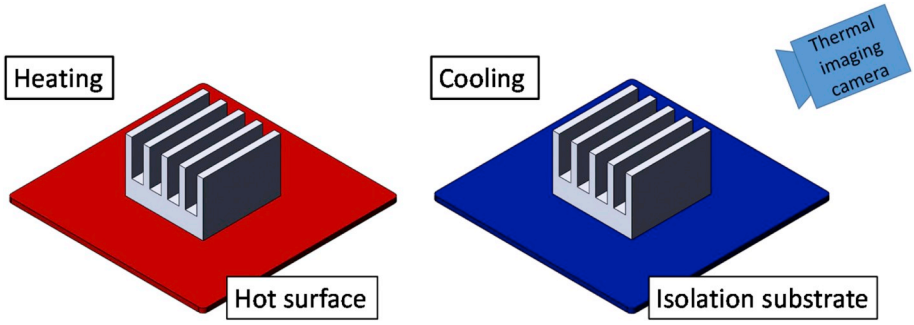

Fig. 4. Illustration of the cooling experiment.

$392 \ll 10^9$, so the flow is laminar.

Under the assumption that the sample has a spatially uniform temperature distribution, the unsteady heat transfer can be described by the lumped system analysis when Biot number (Bi) is much smaller than 0.1 [38]. Biot number $Bi = \frac{hL_C}{k}$ is the ratio between conduction resistance within the fin and the convection resistance at the surface of the fin. For the heatsink geometry, the characteristic length L_C is 0.226 mm. Biot number for aluminum is $Bi \approx 2 \times 10^{-5} \ll 0.1$, with $k_1 = 200$ (W. m^{-1}. K^{-1}). For polymer, $Bi \approx 0.045 < 0.1$ with $k_0 \sim 0.1$ (W. m^{-1}. K^{-1}) is not much smaller than 0.1. Thus, the thermal resistance inside the fin plays a more important role in polymer than in aluminum.

It can be seen from the Biot number analysis, the internal heat conduction resistance needs to be considered, which is comparable to convective thermal resistance. According to the Clausius-Mossotti Approximation (CMA), for a two-component macroscopically isotropic composite medium, with one phase being small spheres (aluminum filler as seen in Fig. 2b as a dilute composites) of conductivity $k_1 = 200$ (W. m^{-1}. K^{-1}), dispersed into a host medium (polymer) of conductivity $k_0 = 0.1$ (W. m^{-1}. K^{-1}), the effective conductivity $\widehat{k}$ can be, $\widehat{k} = \frac{(1+2\omega\nu)k_0}{1-\omega\nu}$. Here, $\omega = \frac{k_1-k_0}{k_1+2k_0} \approx 1$, ν is the concentration of the spheres. That means when adding small amount of filler into polymer randomly, the effective thermal conductivity is very close to the thermal conductivity of the polymer, $\widehat{k} \approx 0.1$(W. m^{-1}. K^{-1}). However, for the case in Fig. 2a, according to the effective medium theory (EMT) [39], considering a 2D two-phase material, with each phase of taking the same area, the effective conductivity can be estimated by geometric mean, $\widehat{k} = \sqrt{k_0 k_1} \approx 4.47$ (W. m^{-1}. K^{-1}). The redistributed assemble fillers can reach the geometric mean at low addition of filler and saved materials.

The transient heat transfer behavior can be estimated by using the lumped system analysis, given by

$$hA_s[T(t) - T_\infty]dt = -\rho C_p V dT \tag{4}$$

where h is the heat transfer coefficient for convection from the entire surface, A_s is the surface area, T_∞ is the ambient temperature, ρ is the density. $T(t)$ denotes that temperature T is a function of time t. Let T_0 be the initial temperature. After applying the initial condition $T(0) = T_0$, the solution of the differential equation in Equation (4) is:

$$T = T_\infty + (T_0 - T_\infty)e^{-\frac{hA_s}{\rho C_p V}t} \tag{5}$$

Put $\theta = \frac{T-T_\infty}{T_0-T_\infty}$, $\tau = \frac{\rho c_p V}{hA_s}$, the solution can be simplified as follows:

$$\theta = e^{-\frac{t}{\tau}} \tag{6}$$

Here, τ is defined as the thermal time constant [40]. A smaller value of τ indicates that the part will approach the surrounding temperature in a shorter time.

4.2. Effects of acoustic redistribution and assembly on composite performance

As a benchmark study, a pure polymer sample U(0,0) is prepared. To study the effects of the acoustic redistribution and assembly of functional fillers on heat dissipation process, uniform composite U(2.75, 2.75) and patterned composite P-1(2.75, 20.5) were fabricated using A-PSL process from the same feedstock which has a filler loading fraction of 2.75 wt%. All manufacturing process parameters were the same for the fabrication of samples U(2.75, 2.75) and P-1(2.75, 20.5), except the curing time and the piezo plate actuation signal. A curing time of 2 s is used for printing the uniform composite layer in sample U(2.75, 2.75). To fabricate sample P-1(2.75. 20.5), 6 s of curing time is needed for solidifying the particle line area, and a sinusoidal signal at 44 kHz with 5 V peak-to-peak voltage is applied to actuate piezo plates for acoustic assembly. The θ was calculated according to the measured temperature, the initial temperature T_0 at 85 °C and the ambient temperature T_∞ at 25 °C. In Fig. 5a, dimensionless temperature θ was plotted as a function of time t. Three replications were performed for temperature measurement of each sample. Three sets of markers represent the average measurements of samples U(0,0), U(2.75, 2.75), and P-1(2.75, 20.5), respectively. The error bar indicates the minimum and maximum measurements in replications. It is evident that the temperature of the part approaches to the ambient temperature exponentially, which agrees with the lumped thermal capacity model.

By fitting the experimental data, the thermal time constant can be obtained, as listed in Table 2. It indicates that the uniform composites took 2.76% less time and the patterned composites took 27.89% less time to cool down, compared to the pure polymer. As shown both in Fig. 5 and Table 2, it is obvious that although a feedstock with a low filler loading fraction (2.75 wt%) is used, the acoustic redistribution and assembly process effectively increased the filler concentration in the fabricated composites, from the 2.75 wt% in the feedstock to 20.5 wt% in the fabricated composite (~8 times increase). Compared to the baseline set by the pure polymer sample U(0,0), the uniform composite U(2.75, 2.75) enhanced the heat dissipation slightly (2.75% enhancement only), due to the low concentration of particles. However, the patterned composite P-1(2.75, 20.5) which was fabricated out of the same feedstock, remarkably enhanced the heat dissipation (27.89% enhancement), due to its highly concentrated particles assembled by the acoustic force in the manufacturing process. Compared to pure polymer, the enhancement of heat dissipation efficiency in the patterned composite is almost 10 times of the enhancement in the uniform composite.

4.3. Effects of multidimensional filler network on composite performance

To highlight the impact of multidimensional filler network on composite thermal performance, samples U(15.4, 15.4), P-2(2.75, 15.4), P-3 (2.75, 15.4), P-4(2.75, 15.4), and P-5(2.75, 15.4) were characterized and compared. They contain the same amount of fillers but have different particle distribution patterns in the polymer matrix. The data

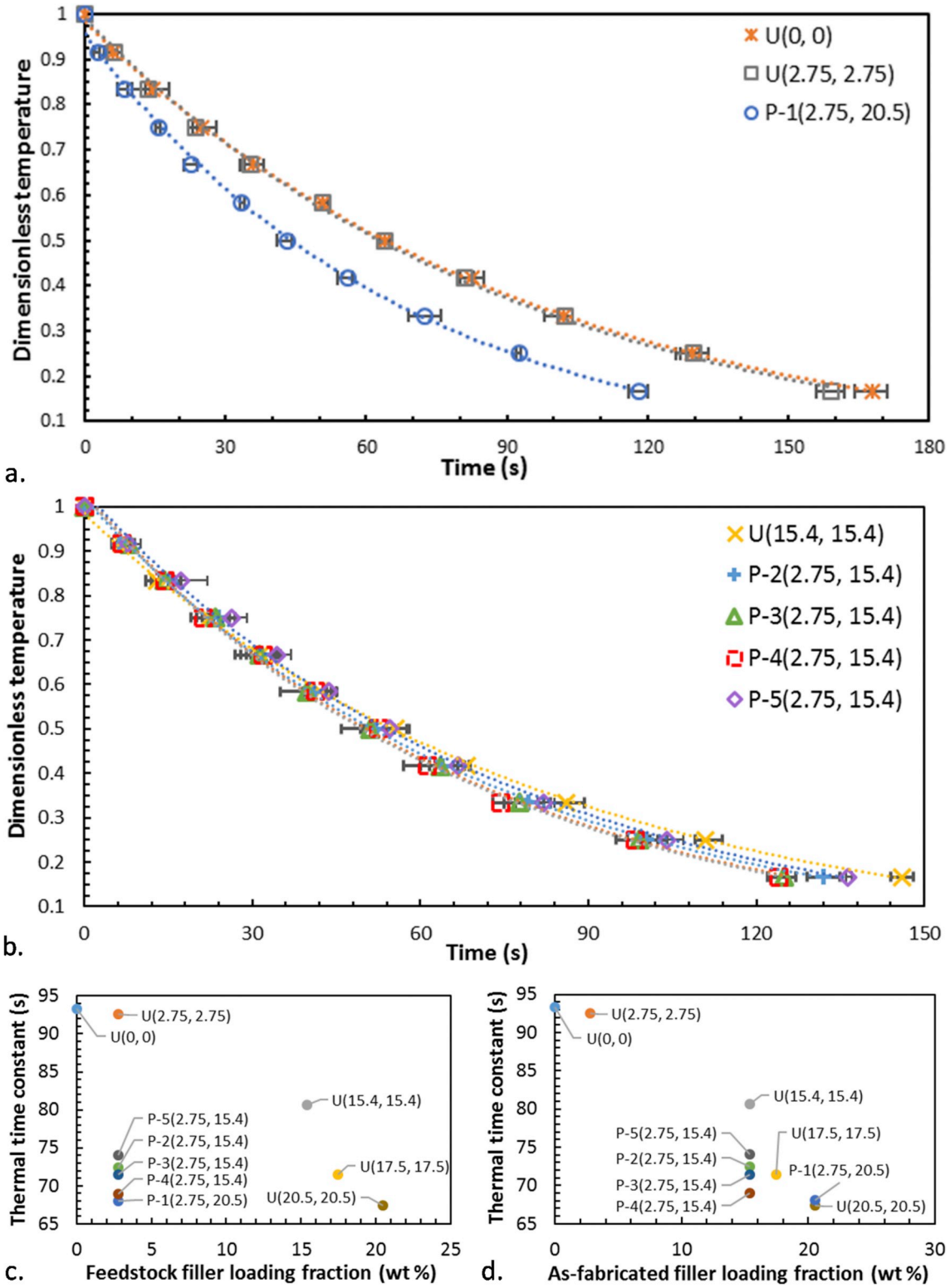

Fig. 5. Heat dissipation of composite samples with: a. Different filler distributions, b. Multidimensional filler networks. Thermal time constants of composite samples versus: c. Feedstock filler loading fraction, and d. As-fabricated filler loading fraction.

collected from cooling experiments were plotted in Fig. 5b. As summarized in Table 2, all patterned composite samples exhibited smaller thermal time constants, compared to the uniform composite U(15.4, 15.4). These differences originate from various designs of the multidimensional filler network in the polymer matrix. It reveals that controlling the filler network construction can adjust the composite heat dissipation ability, without changing the material composition.

Among the four patterned composite samples, the different thermal time constants reflect the impacts of filler network pattern on the composite thermal performance. In sample P-5(2.75, 15.4), a 2D filler network with restricted filler interlayer connection lacks continuous vertical heat transfer path. With 3D filler networks, sample P-4(2.75,

Table 2
Empirical model for printed samples.

Sample	Trend Line Expression	R^2	τ (s)	Enhancement (%)
U(0, 0)	$\theta = 0.98e^{-\frac{t}{94.34}}$	1	94.34	0
U(2.75, 2.75)	$\theta = 0.99e^{-\frac{t}{91.74}}$	0.998	91.74	2.76
P-1(2.75, 20.5)	$\theta = 0.95e^{-\frac{t}{68.03}}$	0.999	68.03	27.89
U(15.4, 15.4)	$\theta = 0.98e^{-\frac{t}{81.30}}$	0.999	81.30	13.82
P-2(2.75, 15.4)	$\theta = 1.02e^{-\frac{t}{72.46}}$	0.999	72.46	23.19
P-3(2.75, 15.4)	$\theta = 1.03e^{-\frac{t}{71.42}}$	0.999	71.42	24.30
P-4(2.75, 15.4)	$\theta = 1.03e^{-\frac{t}{68.97}}$	0.998	68.97	26.89
P-5(2.75, 15.4)	$\theta = 1.03e^{-\frac{t}{74.07}}$	0.998	74.07	21.49
U(17.5, 17.5)	$\theta = 0.98e^{-\frac{t}{72.46}}$	1	72.46	23.19
U(20.5, 20.5)	$\theta = 0.99e^{-\frac{t}{67.43}}$	1	67.43	28.52

15.4) achieved the smallest thermal time constant, which is ~5% less than the one of sample P-5(2.75, 15.4). A possible cause is that the acoustically assembled 3D filler networks surround the isolated pure polymer regions in the sample and provide active heat transfer paths in all dimensions. A smaller isolated region requires less time for heat to transfer. Consequently, samples P-2(2.75, 15.4) and P-3(2.75, 15.4) showed slightly larger thermal time constants, compared to the sample P-4(2.75, 15.4).

4.4. Performance comparison of composites with varied particle filling patterns

To analyze effects of particle concentrations and particle assembly patterns together, the thermal time constants of samples U(17.5, 17.5) and U(20.5, 20.5) were characterized as listed in Table 2, and compared with the previously analyzed samples. Thermal time constants of all samples are plotted according to the feedstock filler loading fraction in Fig. 5c and the as-fabricated filler loading fraction in Fig. 5d.

As shown in Fig. 5c, the as-fabricated filler loading fraction in the uniform composites increases with a higher feedstock filler loading fraction, leading to a drop in the thermal time constant, which means a more efficient heat dissipation. With the same feedstock, patterned composites are composed of much more particles in the form of 2D or 3D network pattern filled in the polymer matrix, resulting in a significant thermal time constant reduction. To fill the same amount of functional particles in the polymer matrix (15.4 wt%), uniform composite U(15.4, 15.4) was fabricated from a feedstock with a 15.4 wt% filler loading fraction, about 6 times higher than the 2.75 wt% feedstock filler loading fraction of patterned composites. However, even with the same amount of particles embedded in samples, four patterned composites P-5(2.75, 15.4), P-2(2.75, 15.4), P-3(2.75, 15.4), and P-4(2.75, 15.4), displayed impressively higher heat dissipation efficiencies than the uniform composite U (15.4, 15.4). Moreover, compared with the uniform composite U(17.5, 17.5) which is filled with 2.1 wt% more particles, the patterned composite P-4(2.75, 15.4) still performs better, as illustrated in Fig. 5d. These comparisons verified the important effects of functional filler assembly on composite heat dissipation efficiency enhancement.

Furthermore, as demonstrated in Fig. 5c and d, although the four patterned composites P-5(2.75, 15.4), P-2(2.75, 15.4), P-3(2.75, 15.4), and P-4(2.75, 15.4) were fabricated out of the same feedstock through the same manufacturing process, and comprise of the same amount of functional fillers, their heat dissipation efficiencies are different, due to different filler spatial distribution patterns. It is clear that the three patterned composites P-2(2.75, 15.4), P-3(2.75, 15.4), and P-4(2.75, 15.4) outperform P-5(2.75, 15.4). The reason is that they possess 3D particle assembly networks rather than 2D network only as in the sample P-5(2.75, 15.4). It proved the effects of filler assembly geometry and dimension on the composite functionality.

As shown in Fig. 5d, the uniform composite U(20.5, 20.5) has a thermal time constant closely matching with the one of P-1(2.75, 20.5), indicating that suspension with a super-low filler loading fraction can be used as feedstock to fabricate composites with the same functionality as the one fabricated out from the feedstock with a heavy filler loading. It implies that the acoustic assembly of highly concentrated continuous filler networks in the polymer matrix can be a promising solution to effective and low-cost productions of functional composites.

5. Conclusions and future work

This work demonstrates the fabrication and design of a novel polymer composite with accelerated heat dissipation. The advanced A-PSL manufacturing technique enables the high design flexibility in the fabrication of polymer composites with programmable filler spatial distribution patterns. The acoustic field directs dispersed fillers to move to specific locations and form into highly concentrated continuous filler networks on the printing plane. Without increasing the filler content in the feedstock, the local filler weight ratio is intensified about 7.5 times within the acoustically assembled microstructures. By controlling the manufacturing parameters, such as the layer thickness and the projection mask, multidimensional filler networks formed. Multidirectional heat transfer paths provided by multidimensional filler networks accelerate the cooling process in the isolated polymer matrix. With the same feedstock or even the same amount of particles filled in the polymer matrix, the patterned composites are superior to the uniform composite with significantly higher heat dissipation efficiencies. Future work will be to quantify the relationship of composite functionality with particle pattern design parameters.

Author disclosure statement

No competing financial interests exist.

Acknowledgements

This material is based upon work partially supported by the National Science Foundation under Grant No.1663399.

Appendix A. Supplementary data

Supplementary data to this article can be found online at https://doi.org/10.1016/j.compositesb.2019.106991.

References

[1] U.S. Air force avionics integrity program notes. 1989.
[2] Mithal P. ASME Design of experimental based evaluation of thermal performance of a flichip electronic assembly in ASME EEP proceedings. New York 1996;18:109–15.
[3] Nikkeshi S, Kudo M, Masuko T. Dynamic viscoelastic properties and thermal properties of Ni powder–epoxy resin composites. J Appl Polym Sci 1998;69(13):2593–8.
[4] Mamunya YP, Davydenko VV, Pissis P, Lebedev EV. Electrical and thermal conductivity of polymers filled with metal powders. Eur Polym J 2002;38:1887–97.
[5] Fu YX, He ZX, Mo DC, Lu SS. Thermal conductivity enhancement with different fillers for epoxy resin adhesives. Appl Therm Eng 2014;66(1–2):493–8.
[6] Tang B, Hu G, Gao H, Hai L. Application of graphene as filler to improve thermal transport property of epoxy resin for thermal interface materials. Int J Heat Mass Transf 2015;85:420–9.
[7] Mun SY, Lim HM, Lee DJ. Thermal conductivity of A silicon carbide/pitch-based carbon fiber-epoxy composite. Thermochim Acta 2015;619:16–9.
[8] Wu Y, Yu Z. Thermal conductivity of in situ epoxy composites filled with Zrb2 particles. Compos Sci Technol 2015;107:61–6.

[9] Yu C, Zhang J, Li Z, Tian W, Wang L, Luo j, Li Q, Fan X, Yao Y. Enhanced through-plane thermal conductivity of boron nitride/epoxy composite. J. Compos. 2017;98:25–31.
[10] Hu J, Huang Y, Yao Y, Pan G. Polymer composite with improved thermal conductivity by constructing a hierarchically ordered three-dimensional interconnected network of BN. ACS Appl Mater Interfaces 2017;9(15):13544–53.
[11] Hong H, Kim JU, Kim T. Effective assembly of nano-ceramic materials for high and anisotropic thermal conductivity in a polymer composite. Polymers 2017;9(9):413.
[12] Gaska K, Rybak A, Kapusta C, Sekula R, Siwek A. Enhanced thermal conductivity of epoxy–matrix composites with hybrid fillers. Polym Adv Technol 2015;26(1):26–31.
[13] Choi SW, Yoon KH, Jeong SS. Morphology and thermal conductivity of polyacrylate composites containing aluminum/multi-walled carbon nanotubes. Composites 2013;45:1–5.
[14] Wattanakul K, Manuspiya H, Yanumet N. Thermal conductivity and mechanical properties of BN-filled epoxy composite: effects of filler content, mixing conditions, and BN agglomerate size. J Compos Mater 2011;45(19):1967–80.
[15] Lee ES, Lee SM, Shanefieldz DJ, Cannon WR. Enhanced thermal conductivity of polymer matrix composite via high solids loading of aluminum nitride in epoxy resin. J Am Ceram Soc 2008;91(4):1169–74.
[16] Burger N, Laachachi A, Ferriol M, Lutz M, Toniazzo V, Rush D. Review of thermal conductivity in composites: mechanisms, parameters and theory. Prog Polym Sci 2016;61:1–28.
[17] Kokkinis D, Schaffner M, Studart AR. Multimaterial magnetically assisted 3D printing of composite materials. Nat Commun 2015;6:8643.
[18] Yang Y, Chen Z, Song X, Zhang Z, Zhang J, Shung KK, Zhou Q, Chen Y. Biomimetic anisotropic reinforcement architectures by electrically assisted nanocomposite 3D printing. Adv Mater 2017;29(11):1605750.
[19] Lu L, Guo P, Pan Y. Magnetic-field-assisted projection stereolithography for three-dimensional printing of smart structures. J Manuf Sci Eng 2017;139(7):071008.
[20] Lu L, Joyee EB, Pan Y. Correlation between micro-scale magnetic particle distribution and magnetic-field-responsive performance of 3D printed composites. J Micro Nano-Manufacturing 2017;6(1):010904.
[21] Lee JW, Ahn G, Kim DS, Cho D-W. Development of nano- and microscale composite 3D scaffolds using PPF/DEF-HA and micro-stereolithography. Microelectron Eng 2009;86(4–6):1465–7.
[22] Hwang S, Reyes EI, Moon K, Rumpf RC, Kim NS. Thermo-mechanical characterization of metal/polymer composite filaments and printing parameter study for fused deposition modeling in the 3D printing process. J Electron Mater 2015;44(3):771–7.
[23] Lewis JA, Smay JE, Stuecker J, Cesarano J. Direct ink writing of three-dimensional ceramic structures. J Am Ceram Soc 2006;89(12):3599–609.
[24] Yuan S, Zheng Y, Chua CK, Yan Q, Zhou K. Electrical and thermal conductivities of MWCNT/polymer composites fabricated by selective laser sintering. Composites Part A 2018;105:203–13.
[25] Lejeune M, Chartier T, Dossou-Yovo C, Noguer R. Ink-jet printing of ceramic micro-pillar arrays. J Eur Ceram Soc 2009;29(5):905–11.
[26] Vrancken B, Thijs L, Kruth JP, Humbeeck JV. Microstructure and mechanical properties of A novel β titanium metallic composite by selective laser melting. Acta Mater 2014;68(15):150–8.
[27] Compton BG, Lewis JA. 3D printing of lightweight cellular composites. Adv Mater 2014;26(34):5930–5.
[28] Decker BY, Gan YX. Electric field-assisted additive manufacturing polyaniline based composites for thermoelectric energy conversion. J Manuf Sci Eng 2015;137(2):024504.
[29] Llewellyn-Jones TM, Drinkwater BW, Trask RS. Printed components with ultrasonically arranged microscale structure. Smart Mater Struct 2016;25(2):02LT01.
[30] Yunus DE, Sohrabi S, He R, Shi W, Liu Y. Acoustic patterning for 3D embedded electrically conductive wire in stereolithography. J Micromech Microeng 2017;27:045016.
[31] Lu L, Tang X, Hu S, Pan Y. Acoustic field-assisted particle patterning for smart polymer composite fabrication in stereolithography. 3D Print Addit Manuf 2018;5(2):151–9.
[32] Sazan H, Piperno S, Layani M, Magdassic S, Shpaisman H. Directed assembly of nanoparticles into continuous microstructures by standing surface acoustic waves. J Colloid Interface Sci 2019;536:701–9.
[33] Petersson F, Aberg L, Swärd-Nilsson A-M, Laurel T. Free flow acoustophoresis: microfluidic-based mode of particle and cell separation. Anal Chem 2007;79(14):5117–23.
[34] Koklu M, Sabuncu AC, Beskok A. Acoustophoresis in shallow microchannels. J Colloid Interface Sci 2010;351(2):407–14.
[35] Pan, Y. Lu, L. Additive manufacturing of magnetic field-responsive smart polymer composites. Proc. ASME 2016 11th International Manufacturing Science and Engineering Conference, I. Ragai, ed., Blacksburg, Virginia, Vol.1, MSEC2016-8865, pp. V001T02A075.
[36] Burger N, Laachachi A, Mortazavi B, Ferriol M, Lutz M, Toniazzo V, Ruch D. Alignments and network of graphite fillers to improve thermal conductivity of epoxy-based composites. Int J Heat Mass Transf 2015;89:505–13.
[37] Burger N, Laachachi A, Ferriol M, Lutz M, Toniazzo V, Ruch D. Review of thermal conductivity in composites: mechanisms, parameters and theory. Prog Polym Sci 2016;61:1–28.
[38] Cengel YA, Ghajar AJ. Heat and mass transfer: fundamentals & applications. fourth ed. New York: the McGraw-Hill Companies, Inc.; 2011.
[39] Mityushev V, Pesetskaya E, Rogosin SV. Cellular and porous materials: thermal properties simulation and prediction, analytical methods for heat conduction in composites and porous media. London: Wiley; 2008. p. 121–64.
[40] Lienhard JHA. Heat transfer textbook. third ed. Cambridge, Massachusetts: Phlogiston Press; 2003.